Environmental Science: Atmospheres

ROYAL SOCIETY OF CHEMISTRY

PAPER

View Article Online
View Journal | View Issue

Cite this: *Environ. Sci.: Atmos.*, 2023, **3**, 1075

Mechanistic study of the complex photooxidation of allyl methyl sulfide (AMS): reaction paths and products of addition under different atmospheric conditions†

Alejandro L. Cardona, [a] María B. Blanco,[a] Mariano A. Teruel*[a] and Oscar N. Ventura *[b]

Received 16th January 2023
Accepted 3rd May 2023

DOI: 10.1039/d3ea00010a

rsc.li/esatmospheres

The addition mechanism of the OH-initiated oxidation of allyl methyl sulfide (AMS) under atmospheric conditions was studied theoretically using both density functional theory (DFT) and the SVECV-f12 composite method. We found that the addition does not occur directly but rather through a pre-reactive complex that serves as a previous stage for addition at both the C1 and C2 positions. However, based on thermodynamics the addition at C2 possibly occurs by branching of the C1 addition mechanism. Once the addition proceeds, the reaction with O_2 under atmospheric conditions produces RO_2 radicals that can decompose in multiple ways. Complex mechanisms of intramolecular rearrangement and decomposition both in the absence and presence of NO_x have been examined. The thermodynamically most favourable decomposition paths produce 2-hydroxy-acetaldehyde, 2-methyl-thio-acetaldehyde, formaldehyde, and the methyl thiomethyl peroxy (**MSP**) intermediate. This latter species is proposed as the main source of sulfur dioxide (SO_2), which is the product found in the highest yield during the experimental determinations.

Environmental significance

Sulfur-containing volatile organic compounds (VOSCs), which can be emitted in significant quantities during the decomposition of organic matter, produce mainly SO_2 during their atmospheric oxidation, a species with the ability to acidify the atmosphere and to form aerosols. Furthermore, in the case of unsaturated sulfides, the degradation mechanism could be extremely complex and gives rise to multiple possible products, some of which are expected and observed, while others are unusual and have not been observed yet. The theoretical study of the reaction mechanisms presented in this paper using high accuracy methods allows for an understanding of how these reactions take place. Moreover, this study opens the exciting possibility of new experimental studies that can lead to identification of new products predicted theoretically.

1 Introduction

Allyl methyl sulfide (AMS) is one of the simplest allyl sulfides, a member of the family of volatile organosulfur compounds (VOSCs), with just a methyl group attached to the sulfur atom. This sulfur containing VOC is emitted into the atmosphere mainly by anaerobic decomposition of organic matter[1,2] and food wastes.[3,4] The gas phase decomposition of VOSCs has important environmental consequences; for instance, they contribute to the acidification of the atmosphere and to aerosol formation.[5] Once in the atmosphere, their main path is the gas phase degradation initiated by OH radicals,[6] as in other unsaturated compounds. This reaction usually initiates *via* addition to the C=C double bond,[7,8] leading to the formation of simpler species.

As in the case of dimethyl sulfide (DMS) degradation, the formation of the methyl thiomethyl radical ($CH_3SCH_2^{\bullet}$) is observed in the oxidation of AMS.[9–11] This radical reacts rapidly with atmospheric O_2 to form methyl thiomethyl peroxy radical (**MSP**, $H_3CSCH_2OO^{\bullet}$).[12] Using electronic structure calculations and RRKM simulations, previous studies showed that an intramolecular H-shift is fast enough to compete with bimolecular reactions under atmospheric conditions.[12,13] Besides, experimental findings reveal a two-step isomerization process of **MSP** radicals, finally forming $HOOCH_2SCHO$ accompanied by OH recycling.[12] In this context, Veres *et al.* recently reported evidence of previously unquantified DMS oxidation product,

[a](L.U.Q.C.A), Laboratorio Universitario de Química y Contaminación del Aire, Instituto de Investigaciones en Fisicoquímica de Córdoba (INFIQC), CONICET, Dpto. de Fisicoquímica, Facultad de Ciencias Químicas, Universidad Nacional de Córdoba, Ciudad Universitaria, 5000 Córdoba, Argentina. E-mail: Mariano.Teruel@unc.edu.ar
[b]Computational Chemistry and Biology Group (CCBG), Detema, Facultad de Química, Universidad de la República, Montevideo, Uruguay. E-mail: Oscar.N.Ventura@gmail.com

† Electronic supplementary information (ESI) available: Optimized geometries and vibrational frequencies of species considered in the AMS oxidation initiated by OH radicals and thermochemistry tables. See DOI: https://doi.org/10.1039/d3ea00010a

hydroperoxymethyl thioformate, from global-scale, airborne observations.[14]

In our recently published experimental work, we determined the rate coefficient of the gas phase degradation of AMS initiated by OH radicals where the main reaction products were detected and quantified.[15] Our findings led us to assume that the degradation mechanism could be more complex than for other unsaturated compounds, due to the presence of the sulfur atom in the molecule. In the case of alkyl sulfides, it has been proposed that in the reaction with OH radicals, those can weakly bind to the sulfur atom, leading to a prereactive complex which has been related to a negative temperature dependence.[16,17] Notwithstanding that high yields of SO_2 were determined, as expected, the formation mechanism of this and other products is not clear enough and the distribution between the mechanisms of addition and abstraction of hydrogen is still uncertain.

Although there are a few theoretical studies on AMS, they mostly aimed to understand gas phase thermal unimolecular decomposition.[18,19] To the best of our knowledge, there are no computational studies on gas-phase degradation initiated by atmospheric radicals. Therefore, in this work we explore in depth the energetics of the addition reaction mechanism involved in the gas phase degradation of AMS initiated by OH radicals using computational methods, to better understand and complement our previous experimental finding o allyl sulfides.[15]

2 Computational details

Geometry optimizations and vibrational analysis of stationary points involved in the gas phase degradation of AMS initiated by OH radicals *via* addition to the C–C double bond were performed using two hybrid exchange–correlation density functional theory (DFT) methods; M06-2X with empirical Grimme dispersion (GD3) and MN15.[20–22] Dunning's cc-pVTZ and aug-cc-pVTZ basis sets were employed for calculations.[23] This is not a random choice. An extensive study of DFT functionals applied to the GMTKN55 database by Goerigk *et al.*[24] showed that dispersion corrected Minnesota functionals are among the top performers, unless one resorts to the much more expensive double hybrid functionals. Since no multiconfigurational species are expected to have relevance in this study, the M06-2X method is appropriate, and the D3 dispersion is necessary, as noted by Goerik *et al.*, even if the original method included part of the dispersion in the determination of the parameters.

For local minima, reactants (R), intermediates (IM), product complexes (PW) and final products (P), the absence of imaginary frequencies was verified. For transition states (TSs), the presence of a single imaginary frequency confirmed that the structures have a translational mode and are maximum w.r.t. the reaction coordinates. Furthermore, intrinsic reaction coordinate (IRC) analyses were performed to confirm that the structure is the correct TS for the path, *i.e.*, that it connects appropriate reactants and products.

In order to get more accurate energies, the recently developed SVECV-f12 composite method was applied.[25] This protocol starts by performing M06-2X-D3 geometry optimization and frequency evaluation. The total energy is then obtained at the optimum geometries by the explicitly correlated CCSDS(T)-F12 method[26,27] extrapolated to the complete basis set limit using the cc-pVDZ-F12 and cc-pVTZ-F12 basis sets.[28] Finally, the core valence correlation energy is calculated by employing the MP2 method with the cc-pVCTZ basis set.[23] The protocol has been tested specifically for the prediction of barriers of reaction for several archetypical systems[25] and found to produce results with an accuracy of 0.5 kcal mol^{-1} or better, in comparison with experiments and/or more sophisticated and expensive methods of calculation.

T1 diagnostics for all the species were checked and found to be $\leq$0.03, indicating that the use of the single-reference method to describe the wave function is appropriate. DFT calculations were performed using the Gaussian 16 software package,[29] while the SVECV-f12 calculations were performed using the Molpro 2020 [30] and ORCA V5.0 [31–33] programs.

3 Results and discussion

We have computationally explored the complete oxidation mechanism of AMS initiated by the OH radical addition to both the α and β positions of the vinyl moiety ($H_2C^{\alpha} = C^{\beta}HR$) labelled as C1 and C2 from now on. Accordingly, C3 is the carbon bonded to C2 and sulfur and C4 is the carbon atom in the methyl group.

Performing an optimized scan using the C2–C3–S–C4 dihedral angle as the dependent variable (while optimizing all the rest of the geometrical parameters, including the C1–C2–C3–S dihedral angle) we found three local minima, as shown in Fig. 1. From these results the difference between the three conformers **AMS_1**, **AMS_2** and **AMS_3** is about 2 kcal mol^{-1} with all the methods used. Since the corresponding isomerization barriers are easily overcome at room temperature, it is reasonable to assume that the three isomers are in equilibrium and ruled by a Boltzmann distribution. Using the best free energies (at the SVECV-f12 level) for the optimized geometries of the three isomers, we obtained relative concentrations of 83%, 5% and 11% respectively (using optimum geometries and the best method of calculation, it was found that **AMS_2** is less stable than **AMS_3** and both are less stable than **AMS_1**). Thus, taking this equilibrium into account, the reaction will proceed from the **AMS_1** isomer preferentially. Therefore, all energies in the following are displayed relative to that of the **AMS_1** isomer. Initially, the results for OH addition and further oxidation leading to products are described assuming that ROO˙ radicals produce RO˙ + O_2 *via* peroxy radical recombination. Then, two alternative routes for the mechanism of decomposition of ROO˙ radicals were explored: the reaction with NO_2 and intramolecular hydrogen migration leading to the formation of OH radicals.

3.1 Addition of OH at C1

Fig. 2 shows the suggested mechanism for the OH radical addition to AMS. Our findings suggest that the addition at C1

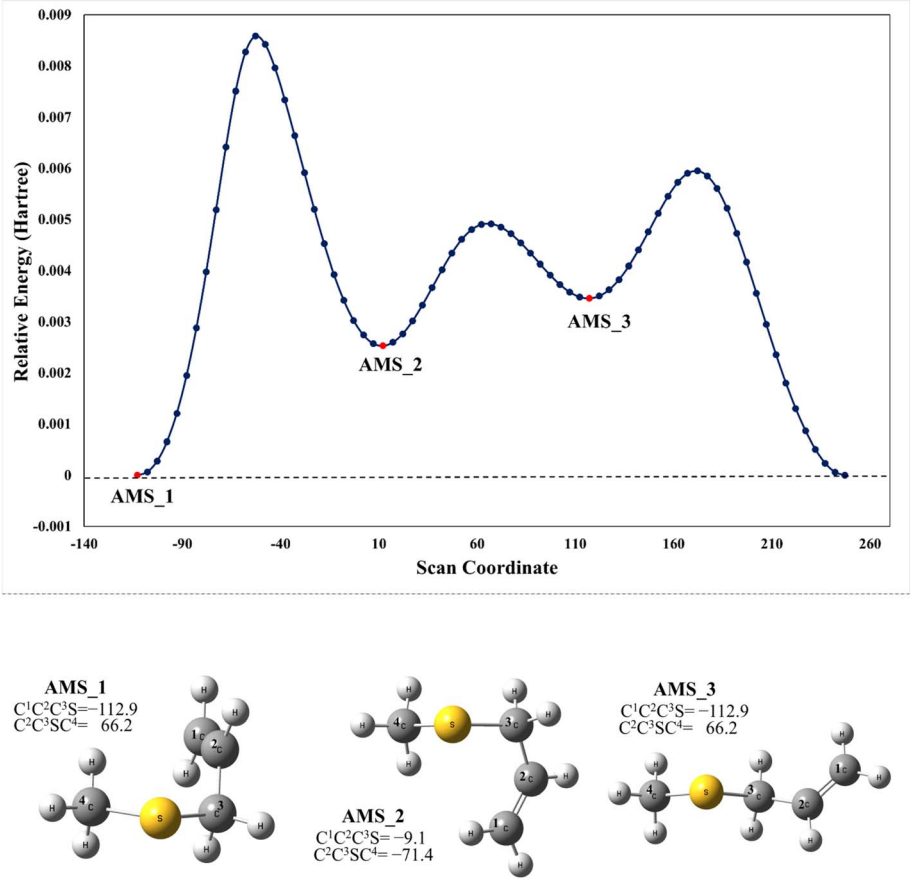

Fig. 1 Upper panel: M06-2X/GD3/aug-cc-pVTZ energy at the optimized geometries on a scan along the C2–C3–S–C4 dihedral angle in AMS. Lower panel: optimized structures of the local minimum energy conformations (*XYZ* coordinates of these and the other structures considered in this paper are compiled in the ESI†).

occurs through a well-defined (but submerged) transition state that is preceded by the formation of a pre-reactive complex (**PRC**) in which the hydroxyl hydrogen interacts with the sulfur atom of the AMS, while the oxygen is positioned towards the double bond and there is no interaction between sulfur and oxygen, forming a dipole–dipole complex as previously reported for DMS.[34] The **PRC** is 4.2, 4.0 and 5.6 kcal mol^{-1} below reactants at the M06-2X-D3/aug-cc-pVTZ, MN15/aug-cc-pVTZ and SVECV-f12 levels of theory, respectively. It is worth mentioning that the **PRC** is an addition complex for both the C1 and C2 positions.

This addition proceeds through **TS1**-C1 which is 2.8 kcal mol^{-1} above the **PRC** but still submerged by 2.8 kcal mol^{-1} relative to reactants forming the intermediate radical **A1** and all the subsequent oxidation steps are submerged relative to the reactants (Fig. 3, the data used to build this graph and the next ones are contained in Tables S2–S5 in the ESI†).

Under atmospheric conditions, the **A1** intermediate can further react with O_2 to produce the peroxy radical **A1O2** (ROO˙). The latter can undergo an isomerization process involving intramolecular hydrogen transfer, leading to products which will be discussed later on (reaction path 2 in Fig. 2). Alternatively, it can be transformed into alkoxy radical **A1O** (RO˙) through three possible routes: (1) a not completely established recombination mechanism involving two molecules of the peroxy radical and further reaction liberating an oxygen molecule (dashed line in Fig. 3), (2) reaction with NO_x (see Section 3.3), or (3) further reaction with OH to produce hydroperoxyl radicals.[35–38] The so formed **A1O** intermediate radical can decompose through the transition state **TS1-1**, breaking the C1–C2 bond, leading to 2-hydroxy-acetaldehyde (**P1**) and the methyl thiomethyl radical ($H_3CSC\cdot H_2$, **Ad_Im1**). Subsequently, **Ad_Im1** reacts further with O_2 to give the **MSP** radical whose decomposition mechanism is well known since it has been studied as part of the DMS oxidation process.[10,12,13,39] We performed anyway a study of the oxidation of this radical at the same level of calculation we used for the rest of the work. The results are described in Section 3.5.

Alternatively, the **A1O** intermediate can decompose by cleavage of the C2–C3 bond through the **TS1-2** transition state. This reaction leads to 2-methyl-thio-acetaldehyde (**P2**), formaldehyde (**P3**), and **HO_2** (see Fig. 2). **P3** is produced by both C1 and C2 addition paths, so it is not useful to characterize this one. **P2** instead would be characteristic of this path, as **P1** was from the reaction through **TS1-1**. However, it should be noted that the formation of **P1** was not experimentally verified by comparing the reference spectrum of **P1** with the post-reaction spectrum of

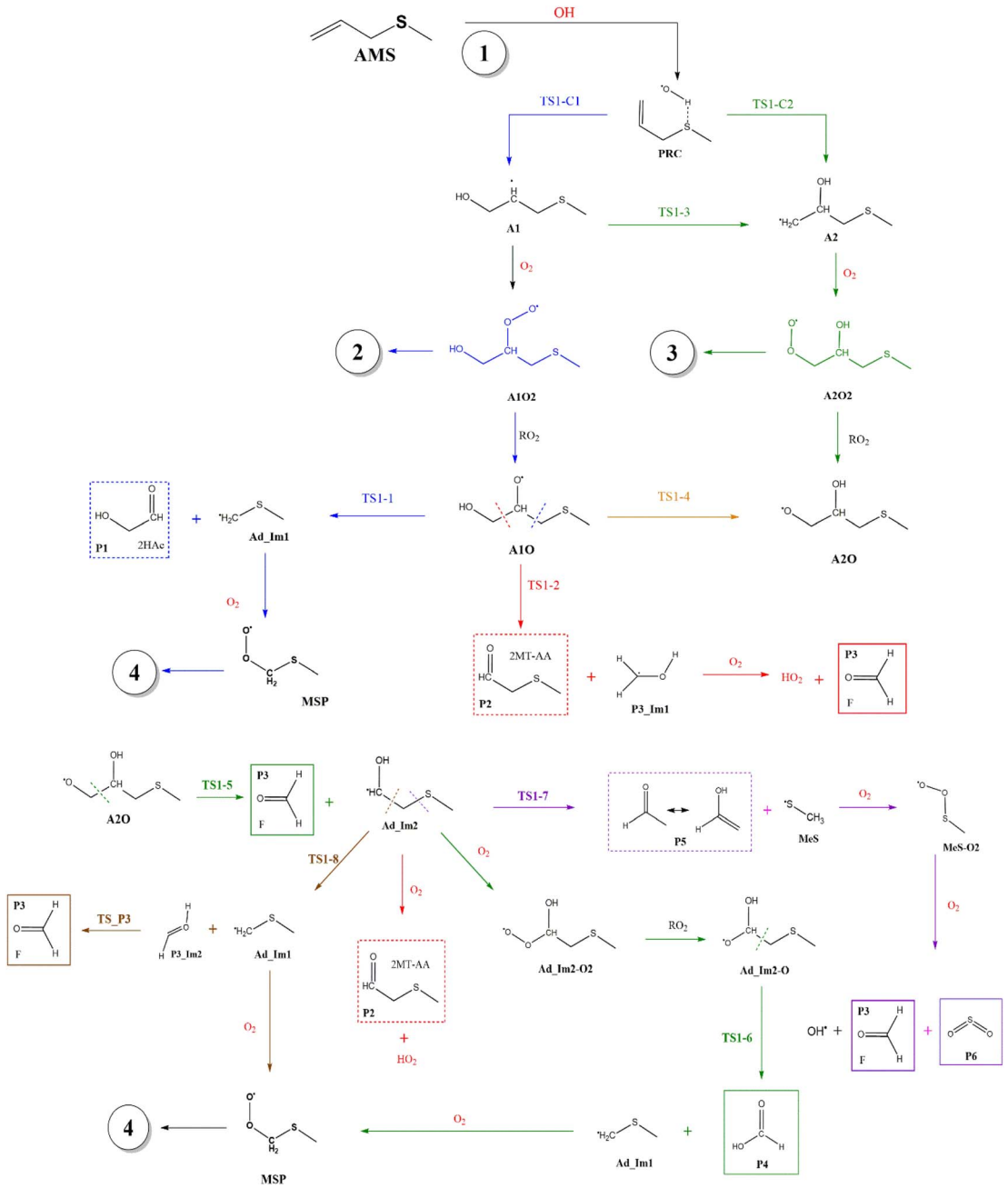

Fig. 2 General mechanism of the OH radical addition to AMS in the absence of NO_x radicals. Products are shown enclosed in boxes: identified (solid lines) and newly proposed (dashed lines).

AMS + OH (see ref. 15). This could mean that it does not form, forms in proportions that are not detectable experimentally, or suffers from secondary processes such as deposition on the walls of the reactor, photolysis, or a reaction with HO_2 radicals which will lead mainly to formaldehyde, formic acid, methanol, CO and OH radicals.[40,41] It can also undergo photoinduced keto–enol isomerization to 1,2-ethenediol *via* the double-hydrogen shift mechanism, which, as has been reported, can be thermodynamically more favorable than photodissociation channels.[42] And, last but not least, the calculated height of the barrier may be too low, although we don't expect the SVECV-f12 protocol to exhibit such an error in the relative energies of **TS1-1** and **TS1-2**. **P2** was not identified experimentally among the products, mainly because of the lack of pure species to measure the IR spectra.

3.2 Addition of OH at C2

As mentioned above, the **PRC** is also a complex for addition to the C2 position through **TS1**-C2 which is slightly submerged at 5.5 kcal mol^{-1} above the **PRC**. However, as part of our search for possible reaction paths we have found **TS1-3**, a transition state connecting **A2** to **A1** (Fig. 4) which is slightly less stable than the

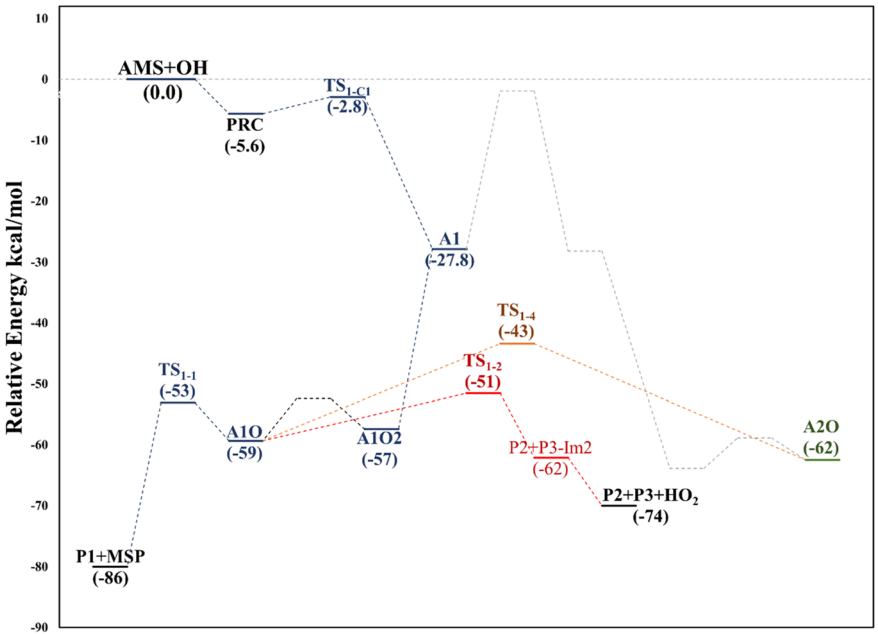

Fig. 3 Partial relative energy diagram for the OH addition to the allyl group in the AMS oxidation initiated by OH radicals at the SVECV-f12 level. Only the addition through **A1** (*i.e.*, the addition of OH at C1 in the absence of NO_x) is shown explicitly.

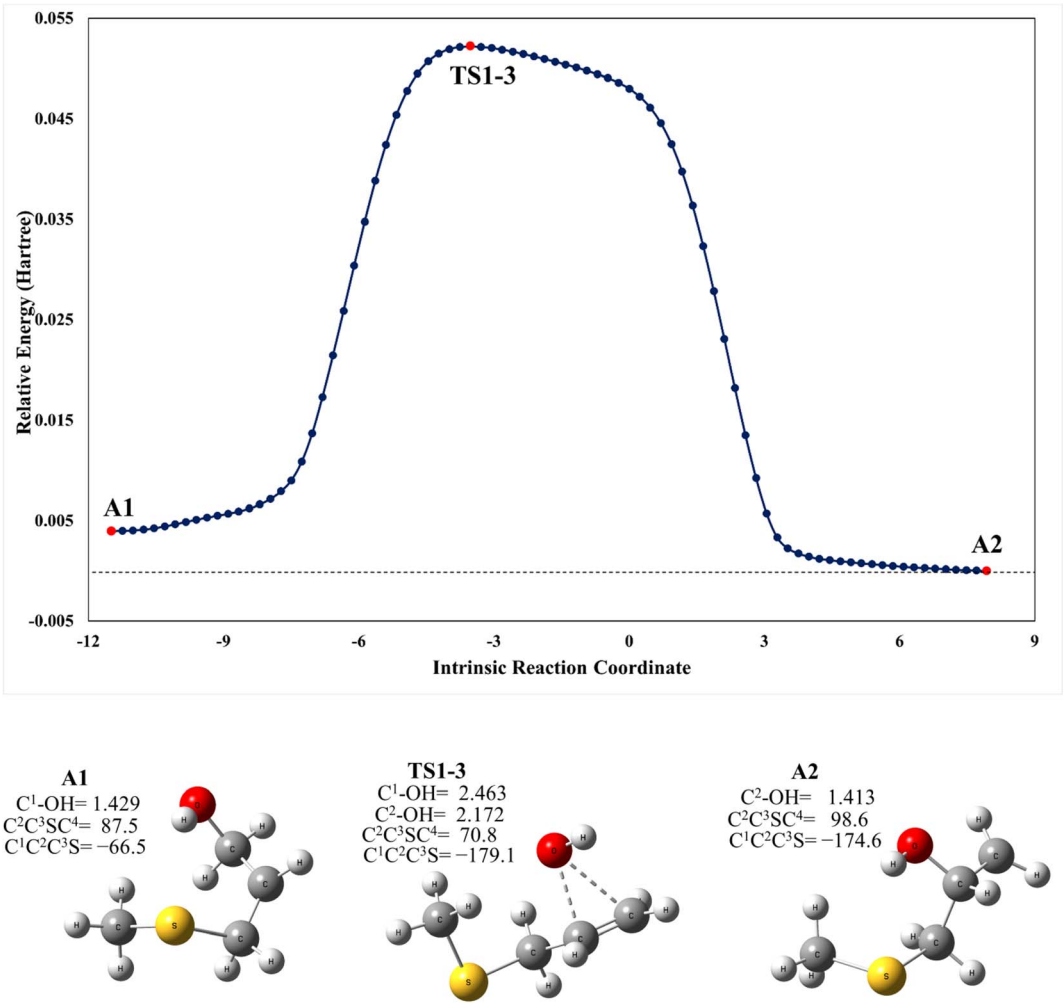

Fig. 4 Upper panel: a plot of intrinsic reaction coordinates for the transition state between the **A1** and **A2** intermediaries, **TS1-3**. Lower panel: optimized structures at the M06-2X/GD3/aug-cc-pVTZ level (*XYZ* coordinates of these species are collected in the ESI†).

former, similarly to what was reported previously for the mechanism of addition of OH to 2-fluoropropene.[43] This finding is consistent with our supposition that an addition mechanism to C2 does not occur directly, but is a branch of the addition path to C1. **TS1-3** is 0.3 kcal mol^{-1} above reactants at the M06-2X-D3/aug-cc-pVTZ level but 1.4 and 1.9 kcal mol^{-1} below them at the MN15/aug-cc-pVTZ and SVECV-f12 levels of theory, respectively. As can be seen in Fig. 4, the IRC in the region of **TS1-3** is considerably flat and broad, indicating the presence of nearly zero eigenvalues, a degenerate condition that explains why **A2** could not be directly reachable from the reactants but nonetheless representing a feasible reaction path.

O_2 addition produces **A2O2** that would eventually generate the **A2O** alkoxy intermediate. In accordance with our assumption, we found another TS that connects the C2 addition path with the addition on C1. **TS1-4** is an H-shift five-member cyclic transition state that goes from **A1O** to **A2O** which has approximately 6 kcal mol^{-1} lower energy. **TS1-4** is below reactants by 45.0, 50.6 and 43.4 kcal mol^{-1} at the M06-2X-D3/aug-cc-pVTZ, MN15/aug-cc-pVTZ and SVECV-f12 levels of theory. Although it seems more likely that the exchange between mechanisms occurs through this TS, the **TS1-4** barrier is approximately 10 kcal mol^{-1} above the **TS1-1** and **TS1-2** transition states that reach products from **A1O** (Fig. 5). **A2O** will release formaldehyde (**P3**) *via* C1–C2 bond cleavage to form the 1-hydroxy-2-(methylthio)-ethyl radical intermediate ($CH_3SCH_2CH^{\bullet}(OH)$, **Ad_Im2**), which can react with O_2 or decompose *via* bond cleavage. The reaction with oxygen can take two paths, H-abstraction to form **P2** and **HO_2** or O_2 addition and recombination to get the alkoxy intermediate, which can in turn decompose to formic acid (**P4**) and **MSP** (prior O_2 addition) *via* **TS1-6**. Bond cleavage between C3 and S through **TS1-7** produces acetaldehyde (or vinyl alcohol, **P5**); further oxidation of the H_3CS intermediate generates sulfur dioxide (**P6**), **P3** and regenerates the OH radical by H-shifting on the H_3CO_2 intermediate. Decomposition through the breaking of the C2–C3 bond produces **MSP** and hydroxy methylene (HC═·═OH, **P3_Im2**) that produce **P3** *via* **TS_P3**. This has not been considered in Fig. 5 since the height of the **TS1-8** barrier is about 10 kcal mol^{-1} above reactants.

Based again on the values collected in Tables S2–S5 in the ESI,† we have collected in Fig. 5 the schematics of the relative energies in the path for the addition of OH at C2, and both paths have been merged and shown in Fig. 6 to have an easier comparison. It is noticeable in Fig. 6 that both paths through intermediaries **A1** and **A2** are in equilibrium. Even if **A2** cannot be obtained directly from the reactants, which prefer to evolve toward **A1**, the transition state for the isomerization is under the reactants (at the best level of calculation) and actually **A2** is slightly more stable than **A1**. The reaction of both intermediaries with O_2 finally produces the radicals **A1O** and **A2O**, with the latter being more stable, and again there is an equilibrium between them with a transition state which is very submerged with respect to reactants.

Both can surmount a small barrier (7–8 kcal mol^{-1}) to give exactly the same products, **P2**, **P3** and **HO_2**. The only fact that makes the real difference is that **A1O** can react further with **P1** and **MSP**, while **A2O** cannot produce **P1**. On the basis of purely thermochemical reasons, it is to be expected that the mechanism of addition to C1 is preferred with the concomitant appearance of **P1** (2-hydroxy acetaldehyde). However, if the barrier of **TS1-4** (which is 9.7 kcal mol^{-1} above **TS1-1** but still

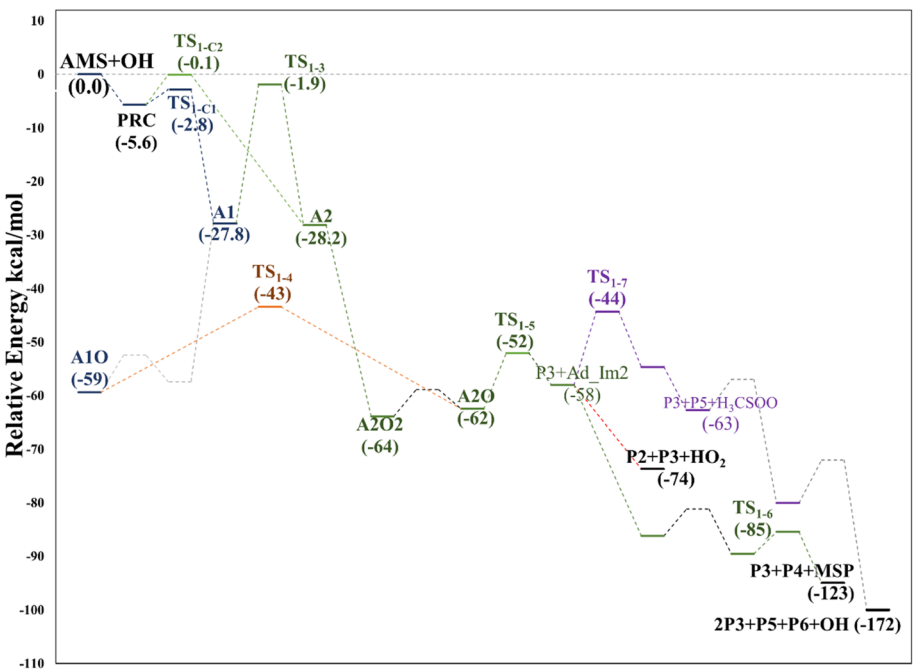

Fig. 5 Relative energy diagram for the OH allyl addition in the AMS oxidation initiated by the OH radical at the SVECV-f12 level. **A2**: addition at C2 in the absence of NO_x.

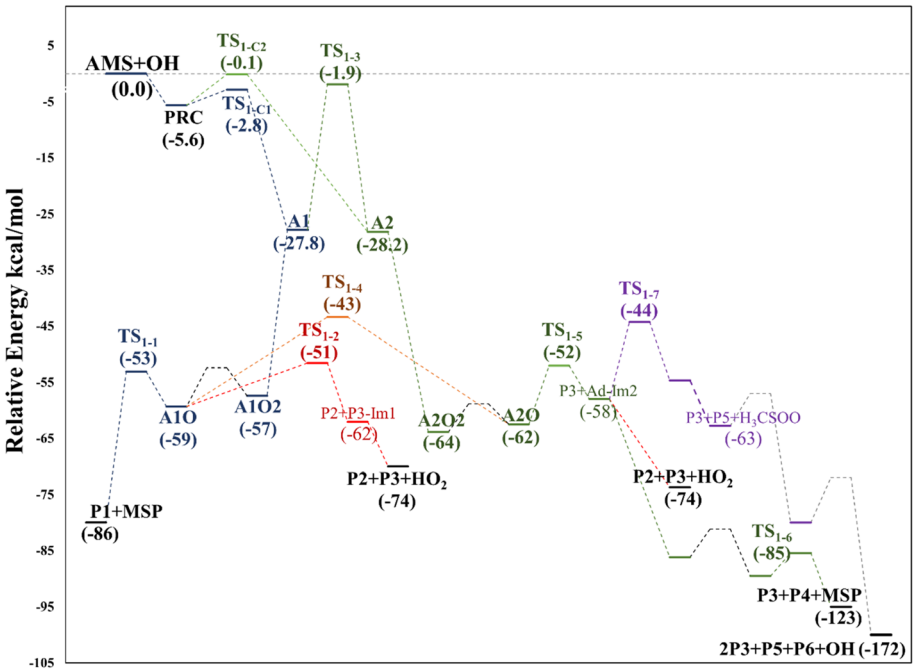

Fig. 6 Relative energy diagram for the OH allyl addition in the AMS oxidation initiated by OH radicals at the SVECV-f12 level. Addition paths in the absence of NO_x.

submerged) is exceeded to get to **A2O**, the latter would produce **P3**, **P4** and **MSP** (−123.3 kcal mol^{-1}) *via* **TS1-5** and **TS1-6** (2.3 and 32.4 kcal mol^{-1} below **TS1-1**) making it a possible and competitive route, supporting the fact that both **P3** and **P4** have been identified experimentally. The reaction of **MSP** ends up producing several reaction products as will be described later.

3.3 Reactions of the peroxy radicals with NO_2

Knowledge of the pathways for the $RO_2^{\bullet} \rightarrow RO^{\bullet}$ transformation is important for radical recycling in the atmosphere. In this section, we explore the formation of alkoxy radicals by the reaction of the peroxy radicals **A1O2** and **A2O2** with NO_2. In our previous experimental work, NO_2 formation was expected when methyl nitrite was used as the precursor of OH radicals (without extra addition of NO). The first step in the reaction with NO_2 of both peroxy radicals is the formation of an organonitrate intermediate ($ROONO_2$). It is actually known that organonitrates can serve as NO_x reservoirs and can make up a significant fraction of secondary organic aerosols (SOAs).[44,45]

The intermediate **A1O2**–NO_2 decomposes directly, forming the alkoxy radical **A1O**. Once NO_3 is released, there is a C2–C3 bond cleavage leading to **P1** and the **Ad_Im1** radical; the latter eventually produces **MSP** by O_2 addition (Fig. 7).

The decomposition of the **A2O2**–NO_2 intermediate occurs through a six-member intermolecular H-abstraction TS, which is 48.6 and 57.0 kcal mol^{-1} below reactants and 36.3 and 33.5 kcal mol^{-1} above **A2O2**–NO_2 at the M06-2X-D3/aug-cc-pVTZ and MN15/aug-cc-pVTZ levels of theory, respectively. We calculated in this study that $\mathbf{TS_{NOx}}$ leads to HNO_3 (**P7**) and 2-hydroxy-3-methylthio-propanaldehyde (**P8**). However, these products have not been observed experimentally yet. The relative energies in this process are shown in Fig. 8.

3.4 Intramolecular rearrangement mechanism in RO_2 intermediates

Based on the experimental and theoretical studies for the **MSP** radical.[12–14] we have investigated the similar internal rearrangement mechanism for the RO_2 radicals formed in the oxidation of AMS, since there are five possible positions for internal H-abstraction, which may reveal new pathways and reaction products. The scheme with the possible paths is represented in Fig. 9.

3.4.1 A1O2. The peroxy radical **A1O2** is formed when the OH addition takes place on C1 and the O_2 molecule adds at C2. We found three stable conformations for **A1O2** called **A1_Im1**, **A1_Im2** and **A1_Im3**, whose only difference lies in how the $HOCH_2CHR(OO^{\bullet})$ moiety is arranged. In **A1_Im1** the peroxy radical points toward the H atom of the OH group at C1, the value of dihedral angles HO–C1–C2–OO$^{\bullet}$ and $^{\bullet}$OO–C2–C3–S is −81.7 and 54.0°, and the bond lengths O–HO and O–S are 2.188 and 3.190 Å, respectively. This leads to two different ways of internal rearrangement: addition to the sulfur atom or H-migration from the OH group to the ROO$^{\bullet}$ moiety. Addition to the sulfur atom generates the **A1_Im1_1** intermediate through a five member TS (**TS2-1**), at 23.1 kcal mol^{-1} below the reactants and 37.2 kcal mol^{-1} above **A1_Im1** (see Fig. 9). In this species the O–S and C3–S distances are 1.733 and 2.293 Å, respectively. The next step in this path is **A1_Im1_1** decomposition *via* C2–O bond scission to produce 2-propenol (**P9**) and the $CH_3SOO^{\bullet}$ radical. After S–C cleavage and further oxidation, the radical

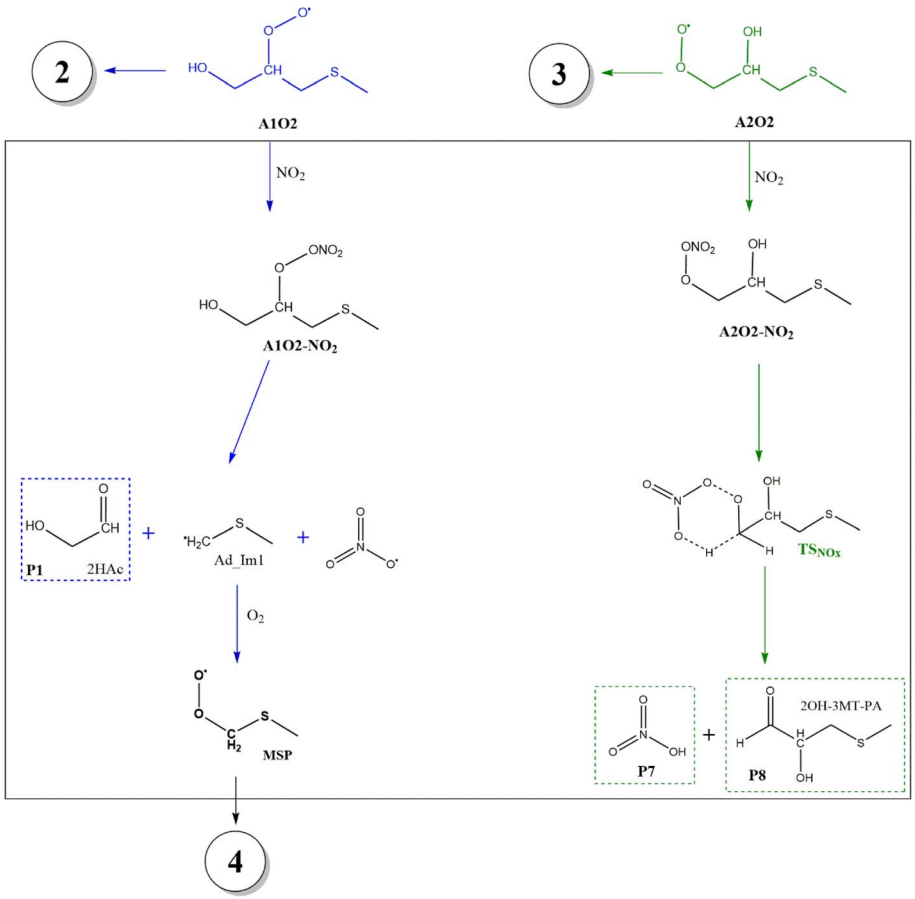

Fig. 7 General mechanism for decomposition of RO_2 radicals formed in the AMS oxidation initiated by OH radicals in the presence of NO_x. Proposed products are shown enclosed in dashed line boxes.

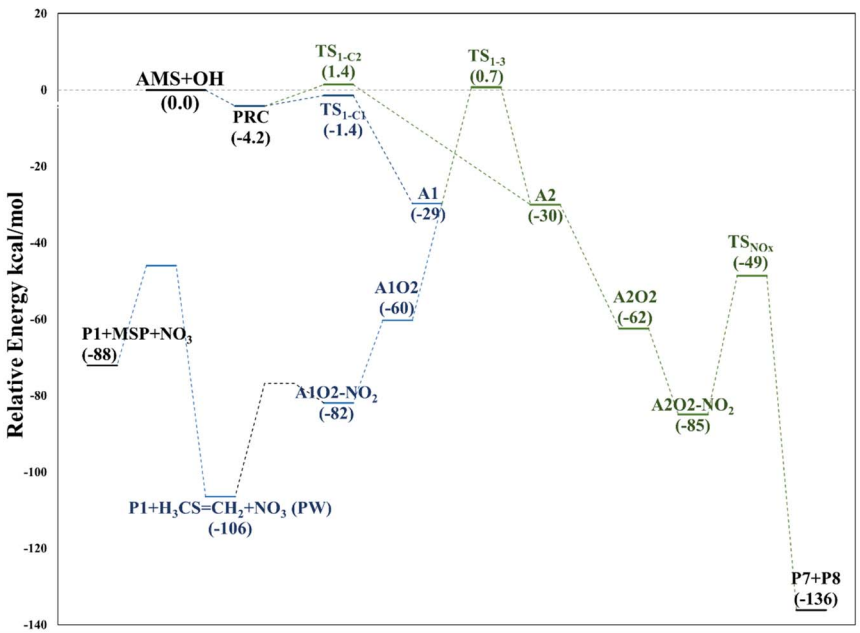

Fig. 8 Relative energy diagram for decomposition of RO_2 radicals formed in the AMS oxidation initiated by OH radicals in the presence of NO_x at the M06-2X/GD3/aug-cc-pVTZ level.

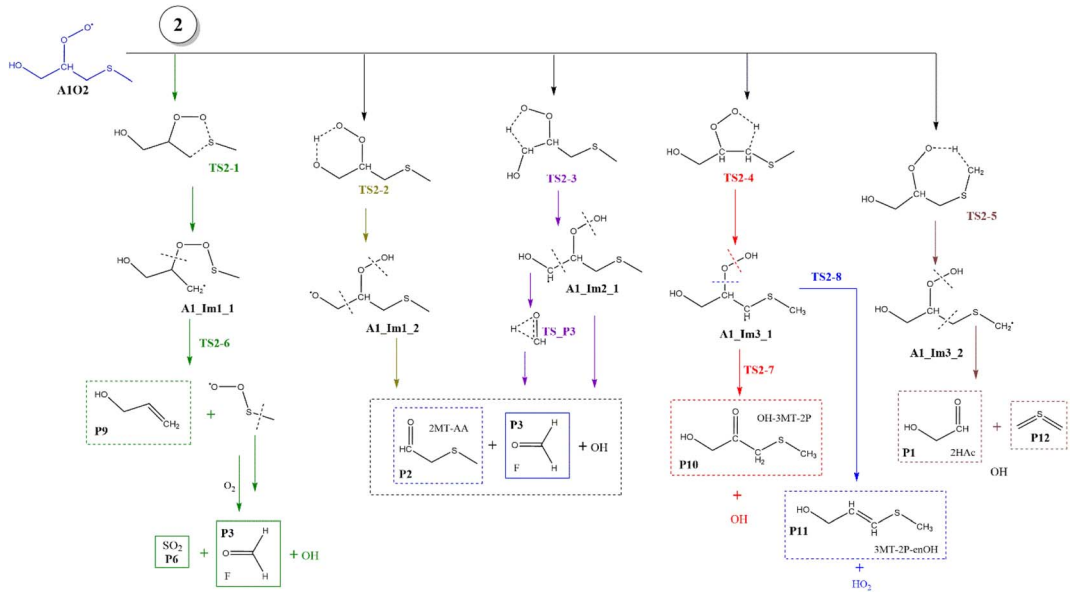

Fig. 9 General mechanism of **A1O2** intermediate (addition to C1) decomposition in the absence of NO_x. Products are shown enclosed in boxes: identified (solid line) and proposed (dashed line).

$CH_3SOO^{\bullet}$ would produce sulfur dioxide (**P6**, experimentally observed), **P3** and OH radical regeneration. H-migration occurs through a six-member TS (**TS2-2**) in which the O–HO is reduced to 1.088 Å. The barrier of **TS2-2** from **A1_Im1** is 23.0 kcal mol^{-1} and −37.2 kcal mol^{-1} relative to reactants (see Table S2†). The decomposition of the **A1_Im1_2** intermediate leads to **P2** and **P3** and again to the OH radical.

The internal H-migration from C1 to ROO$^{\bullet}$ occurs from the **A1_Im2** intermediate. In this structure the value of the HO–C1–C2–OO$^{\bullet}$ dihedral angle is 175.0°, leaving the HO and ROO$^{\bullet}$ groups in opposite directions. The ROO$^{\bullet}$–HC1 distance in the **A1_Im2** intermediate is 2.550 Å and the abstraction proceeds through a five-member cyclic TS (**TS2-3**) in which that distance is reduced to 1.290 Å to obtain the **A1_Im2_1** intermediate. The barrier for this process is 26.5 kcal mol^{-1} from **A1_Im2** and 33.1 kcal mol^{-1} below reactants (Table S2†). Once the **A1_Im2_1** intermediate decomposes, it generates **P2**, the OH radical and the HCOH species that eventually produces **P3** (see Fig. 9).

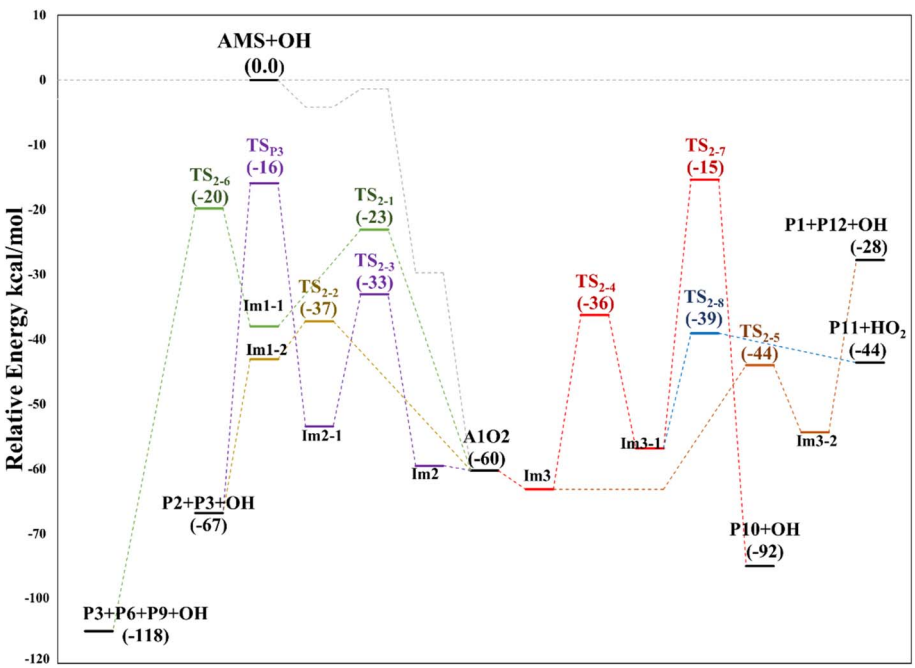

Fig. 10 Relative energy diagram for decomposition of the **A1O2** intermediate (addition to C1) formed in the AMS oxidation initiated by OH radicals in the absence of NO_x at the M06-2X/GD3/aug-cc-pVTZ level.

Finally, from the **A1_Im3** intermediate, the internal H-abstraction could occur at the C3 and C4 positions. Abstraction at C3 produces **A1_Im3_1** through a five-member cyclic TS (**TS2-4**) which is 27.0 kcal mol^{-1} above **A1_Im3**. The **A1_Im3_1** intermediate could decompose into two sets of products, OH radicals and hydroxy-3-methylthio-2-propanone (**P10**) by O–O bond cleavage or **HO_2** radicals and 3-methylthio-2-propenol (**P11**) by C–O bond cleavage. Instead, the abstraction at the C4 position (methyl group) goes through a cyclic TS (**TS2-5**) with a barrier of 19.2 kcal mol^{-1} which is the lowest in the **A1O2** mechanism (Table S2†). Intermediate **A1_Im3_2** decomposes to **P1** and thioformaldehyde-*S*-methylide (**P12**).[34,46–48] The energies of all these processes are schematized in Fig. 10.

3.4.2 A2O2. If the mechanism follows the path of C2 addition as described previously, the O_2 addition to **A2** produces the **A2O2** intermediate. This species exhibits two different conformations which we called **A2_Im1** and **A2_Im2**. We have found three different mechanisms for internal H-abstraction in the CH and OH groups at C2 and in the CH group at C3 (see Fig. 11).

In all paths, the internal H-abstraction produces an intermediate with the $HOOCH_2R$ form, and eventually the $HOOCH_2$- moiety ends up giving OH radicals and **P1**. Both internal H-abstractions at C2 will also produce **P2** through the transition states **TS3-1** and **TS3-2**, whose barriers are 29.3 and 19.3 kcal mol^{-1} relative to **A2_Im1**, respectively (Table S3†). However, to obtain **P2** from the $^{\bullet}C(HO)CH_2SCH_3$ radical formed in R3-1 (**P2_Im1**), it is necessary to reach a high energy barrier of 10.9 kcal mol^{-1} above the reactants (**TS3-5**), not a plausible process. Internal H-abstraction from C3 goes through the transition state **TS3-3**, which has a barrier of 20.6 kcal mol^{-1} relative to **A2_Im2**. Final products of this path are **P1**, OH, and 2-methylthioethanol (**P13**). The energy schematics are shown in Fig. 12.

3.5 MSP decomposition

Although the radical decomposition mechanism of **MSP** is generally well explored, in this section we report an in depth study of all possible degradation pathways at the same level of calculation as we treated the rest of the mechanism, including intramolecular rearrangement and H-shift paths (Fig. 13). The best-known path for **MSP** decomposition is recombination to the corresponding alkoxy radical **MSO** and C–S bond cleavage to form **P3** and the methylthiyl radical ($CH_3S^{\bullet}$). The $CH_3S^{\bullet}$ radical can either dimerize to dimethyl disulfide (**DMDS**) or form the methylthiyl peroxy radical ($CH_3SOO^{\bullet}$) by adding oxygen; the latter then produces another **P3** molecule and **P6** by S–C bond cleavage. Both the formation of **DMDS** and **P3** + **P6** paths occur with low barriers once recombination of RO_2 radicals occurs (Fig. 14).

However, as previously addressed both theoretically and experimentally,[12,13,49] in the absence of NO_x and at low concentrations of **HO_2** or RO_2 radicals, the **MSP** isomerization path could be competitive with bimolecular reactions. The first isomerization step *via* internal H-abstraction has a barrier of approximately 20 kcal mol^{-1} (energies relative to **MSP** in this section) and proceeds through a cyclic TS (**TS4-1**) in which the

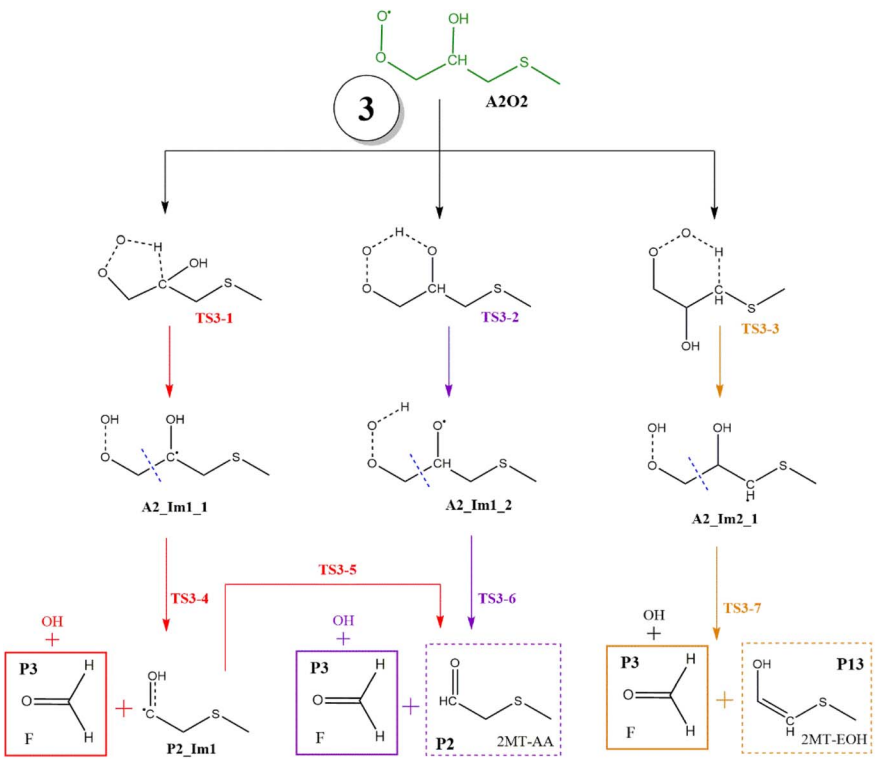

Fig. 11 General mechanism of A2O2 intermediate (addition to C2) decomposition in the absence of NO_x. Products are shown enclosed in boxes: identified (solid line) and proposed (dashed line).

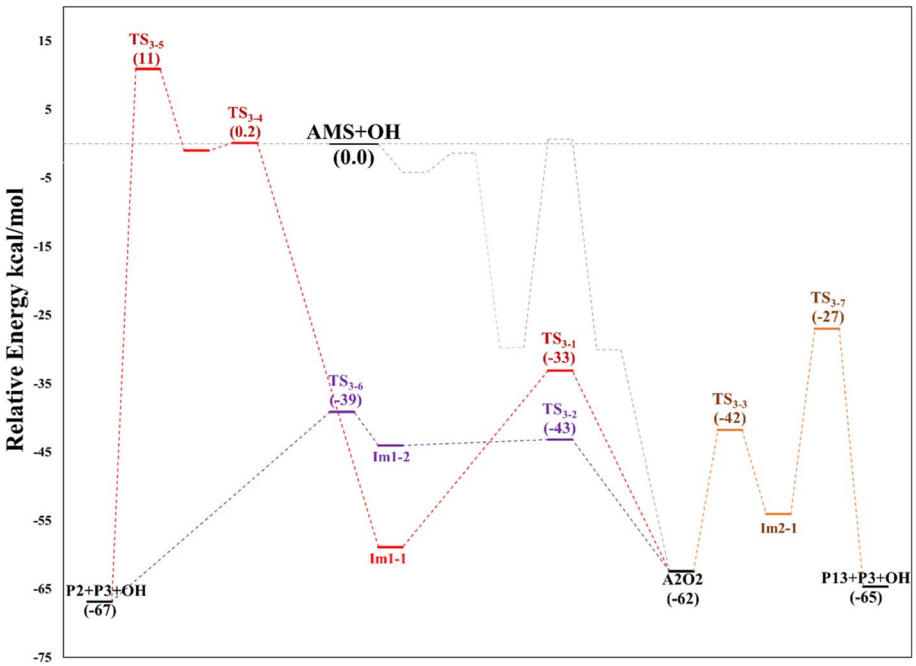

Fig. 12 Relative energy diagram for decomposition of the A2O2 intermediate (addition to C2) formed in the AMS oxidation initiated by OH radicals in the absence of NO_x at the M06-2X/GD3/aug-cc-pVTZ level.

hydrogen moves from the methyl group to the ROO˙ moiety to generate the **MSP-1** intermediate. **MSP-1** produces **P3**, thioformaldehyde (**P14**) and the OH radical if the reaction proceeds *via* S–C bond cleavage (**TS4-2**), with a barrier of 25 kcal mol^{-1} relative to **MSP-1**. However, although the **MSP-1** intermediate is 9 kcal mol^{-1} above **MSP**, the reaction with O_2 is barrierless and forms **MSP-2**, which was already detected experimentally by Berndt *et al.*[12] and is 17.4 kcal mol^{-1} below **MSP** (Fig. 14).

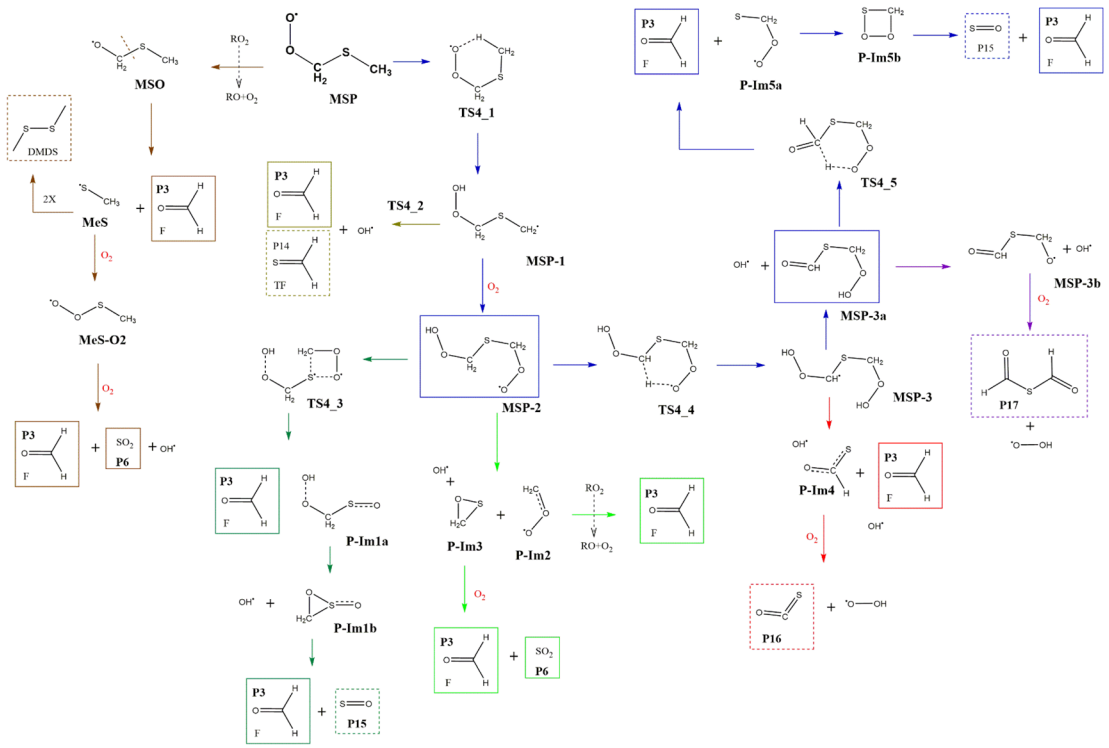

Fig. 13 General mechanism of MSP intermediate decomposition in the absence of NO_x. Products are shown enclosed in boxes: identified (solid line) and proposed (dashed line).

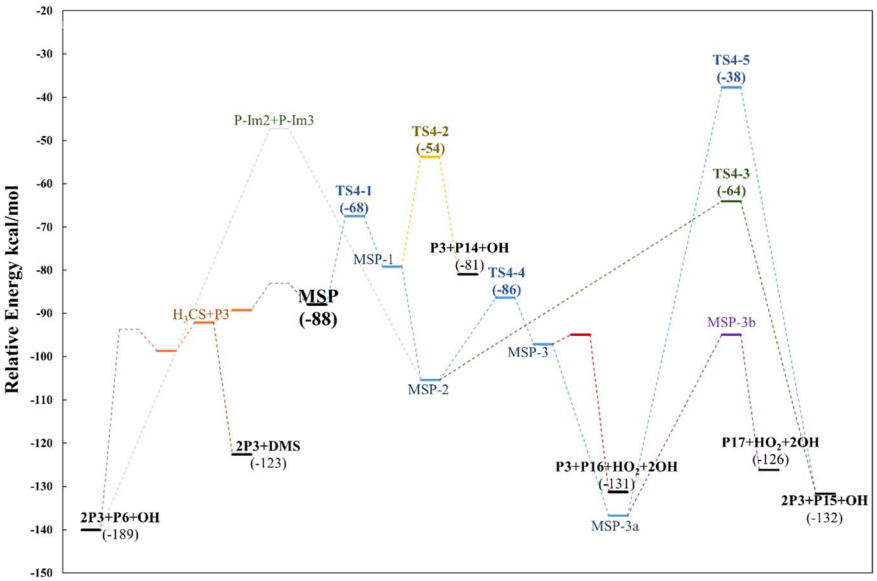

Fig. 14 Relative energy diagram for decomposition of the **MSP** intermediate formed in the AMS oxidation initiated by OH radicals in the absence of NO_x at the M06-2X/GD3/aug-cc-pVTZ level.

Both energies calculated using the SVECV-f12 protocol for **TS4-1** and **MSP-1**, −5.1 and −17.3 kcal mol^{-1} respectively, (relative to $CH_3SOO^{\bullet}$ + O_2), are in good agreement with those obtained at the UCBS-QB3, ROCBS-QB3, and M06-2X levels by Wu *et al.*[13] However, their energies at the UCBS-QB3 (1.5 kcal mol^{-1}) and ROCBS-QB3 (2.3 kcal mol^{-1}) levels for **TS4-2** disagree with that predicted by themselves at the M06-2X level (9.1 kcal mol^{-1}) and with what we obtained using the SVECV-f12 protocol (8.0 kcal mol^{-1}) relative to $CH_3SOO^{\bullet}$ + O_2.

MSP-2 can produce two molecules of **P3**, OH radical and sulfur monoxide (**P15**) through the transition state **TS4-3** (41.2 kcal mol^{-1}), decompose by breaking the S–C bond, forming two molecules of **P3** and one of **P6**, or can undergo an internal hydrogen migration (through **TS4-4**, at 19.0 kcal mol^{-1}) generating the **MSP-3** intermediary which decomposes to **P3**, carbonyl sulfide (**P16**), and **HO_2** releasing two OH radicals. OH loss from **MSP-3** is highly exothermic and produces the **MSP-3a** intermediate, which was also detected experimentally by Berndt *et al.*[12] **MSP-3a** can then decompose by two different paths in which one OH radical is released for each molecule of the intermediate: (i) decomposition to **P17** and **HO_2** or (ii) formation of two molecules of **P3** and one of **P15** by intermolecular migration of H (**TS4-5**, 99.1 kcal mol^{-1}). Wu *et al.*[13] also proposed the reaction of **MSP-3a** with OH radicals.

Since all transition states are submerged by many kcal mol^{-1}, all paths are kinetically open, but from a thermodynamic point of view, the route leading to 2**P3** + **P6** is clearly favoured, which agrees with the products observed experimentally. However, it is not implausible that variation in the experimental conditions could lead to other products, of which the one that looks more interesting is formic thioanhydride (**P17**).

4 Conclusions

As usual for unsaturated compounds, addition to the double bond in the OH-initiated oxidation of AMS is an important decomposition pathway. Although AMS has two possible OH addition positions, the results obtained in this work lead us to assume that the addition does not occur directly but rather through a pre-reactive complex that serves as a previous stage for addition at both the C1 and C2 positions. Based on the energetics of the TSs for the addition pathways, it is also possible to suggest that the addition at C2 could be a branch of the C1 addition mechanism. The addition path to C1 generates 2-hydroxy-acetaldehyde (**P1**), 2-methyl-thio-acetaldehyde (**P2**), formaldehyde (**P3**), and the intermediate methyl thiomethyl peroxy (**MSP**) radical. If the reaction follows the path in which the OH is attached to C2 instead, the mechanism is more complex. **P2**, **P3**, formic acid (**P4**), acetaldehyde (**P5**), sulfur dioxide (**P6**) and the intermediate **MSP** are generated.

In the oxidation initiated by OH, independent of whether at C1 or C2, secondary RO_2 radicals are formed by a reaction with oxygen. Further reactions of these radicals with NO_2 molecules (simulating polluted atmospheres) and the intramolecular rearrangement implying internal H-shift and subsequent oxidations (pristine atmospheres) were proposed. The energetics and degradation mechanisms of these pathways suggest that it is possible that, in addition to the experimentally identified products, more complex sulfide compounds may be formed, but have not been detected yet. The **MSP** intermediate decomposition is the main source of sulfur dioxide (**P6**), which is the product found with the highest yield during the AMS experimental determinations. Again, intramolecular rearrangement and successive oxidations open up a range of new

pathways that are thermodynamically accessible and generate products that have not been previously proposed.

In this work, two different levels of theory have been used: DFT and the recently developed SVECV-f12 composite method. Although the results in general show good agreement, thus validating in general the use of DFT methods, some differences were observed in the reaction barrier values, whose accuracy is essential for the calculation of theoretical rate coefficients. Additional calculations for the H abstraction mechanism are currently being carried out to determine rate constants for both oxidation paths (double bond addition and H abstraction) in order to obtain an overall rate constant that allows a full comparison between the theoretical and experimental results.

Conflicts of interest

There are no conflicts to declare.

Acknowledgements

A. L. C. acknowledges CONICET (Argentina) for a doctoral fellowship and support. M. B. B. wishes to acknowledge the Alexander von Humboldt Foundation for the support. M. T. acknowledges FONCYT (Argentina), SECYT (Argentina), and CONICET (Argentina) for financial support of this research. O. N. V. thanks Pedeciba (Uruguay), CSIC (Uruguay) and ANII (Uruguay) for continuing support to the research in their group. Calculations reported in this paper were carried out using ClusterUY (site: **https://www.cluster.uy**), the cluster at the CCBG (Uruguay) and at the CCAD-UNC, which is part of SNCAD-MinCyT, Argentina. The authors want to thank the reviewers for the careful reading that allowed us to improve the quality and clarity of the manuscript.

References

1 T. Wu, X. Wang, D. Li and Z. Yi, Emission of volatile organic sulfur compounds (VOSCs) during aerobic decomposition of food wastes, *Atmos. Environ.*, 2010, **44**, 5065–5071.

2 A. Muezzinoglu, A study of volatile organic sulfur emissions causing urban odors, *Chemosphere*, 2003, **51**, 245–252.

3 H.-X. Cao, K.-X. Zhu, J.-G. Fan and L. Qiao, Garlic-Derived Allyl Sulfides in Cancer Therapy, *Anti-Cancer Agents Med. Chem.*, 2014, **14**, 793–799.

4 A. K. Sinha, S. A. Farooqui, A. Sharma, A. Mishra and V. Verma, Reactivity of allyl methyl sulphide, the in vitro metabolite of garlic, with some amino acids and with phospholipid involved in viral infections, *J. Biomol. Struct. Dyn.*, 2022, **40**, 565–571.

5 R. J. Charlson, J. E. Lovelock, M. O. Andreae and S. G. Warren, Oceanic phytoplankton, atmospheric sulphur, cloud albedo and climate, *Nature*, 1987, **326**, 655–661.

6 B. J. Finlayson-Pitts and J. N. Pitts Jr, *Chemistry of the Upper and Lower Atmosphere: Theory, Experiments, and Applications*, Elsevier, 1999.

7 M. P. Walavalkar, S. Vijayakumar, A. Sharma, B. Rajakumar and S. Dhanya, Is H Atom Abstraction Important in the Reaction of Cl with 1-Alkenes?, *J. Phys. Chem. A*, 2016, **120**, 4096–4107.

8 C. Pfrang, M. D. King, C. E. Canosa-Mas and R. P. Wayne, Structure-activity relations (SARs) for gas-phase reactions of NO_3, OH and O_3 with alkenes: an update, *Atmos. Environ.*, 2006, **40**, 1180–1186.

9 I. Barnes, K. H. Becker and I. Patroescu, FTIR product study of the OH initiated oxidation of dimethyl sulphide: observation of carbonyl sulphide and dimethyl sulphoxide, *Atmos. Environ.*, 1996, **30**, 1805–1814.

10 M. Albu, I. Barnes, K. H. Becker, I. Patroescu-Klotz, R. Mocanu and T. Benter, Rate coefficients for the gas-phase reaction of OH radicals with dimethyl sulfide: temperature and O2 partial pressure dependence, *Phys. Chem. Chem. Phys.*, 2006, **8**, 728–736.

11 I. Barnes, V. Bastian and K. H. Becker, Kinetics and mechanisms of the reaction of OH radicals with dimethyl sulfide, *Int. J. Chem. Kinet.*, 1988, **20**, 415–431.

12 T. Berndt, W. Scholz, B. Mentler, L. Fischer, E. H. Hoffmann, A. Tilgner, N. Hyttinen, N. L. Prisle, A. Hansel and H. Herrmann, Fast Peroxy Radical Isomerization and OH Recycling in the Reaction of OH Radicals with Dimethyl Sulfide, *J. Phys. Chem. Lett.*, 2019, **10**, 6478–6483.

13 R. Wu, S. Wang and L. Wang, New mechanism for the atmospheric oxidation of dimethyl sulfide. The importance of intramolecular hydrogen shift in a CH3SCH2OO radical, *J. Phys. Chem. A*, 2015, **119**, 112–117.

14 P. R. Veres, J. Andrew Neuman, T. H. Bertram, E. Assaf, G. M. Wolfe, C. J. Williamson, B. Weinzierl, S. Tilmes, C. R. Thompson, A. B. Thames, J. C. Schroder, A. Saiz-Lopez, A. W. Rollins, J. M. Roberts, D. Price, J. Peischl, B. A. Nault, K. H. Møller, D. O. Miller, S. Meinardi, Q. Li, J. F. Lamarque, A. Kupc, H. G. Kjaergaard, D. Kinnison, J. L. Jimenez, C. M. Jernigan, R. S. Hornbrook, A. Hills, M. Dollner, D. A. Day, C. A. Cuevas, P. Campuzano-Jost, J. Burkholder, T. Paul Bui, W. H. Brune, S. S. Brown, C. A. Brock, I. Bourgeois, D. R. Blake, E. C. Apel and T. B. Ryerson, Global airborne sampling reveals a previously unobserved dimethyl sulfide oxidation mechanism in the marine atmosphere, *Proc. Natl. Acad. Sci. U. S. A.*, 2020, **117**, 4505–4510.

15 A. L. Cardona, R. G. Gibilisco, C. B. Rivela, M. B. Blanco, I. Patroescu-Klotz, N. Illmann, P. Wiesen and M. A. Teruel, Kinetics, product distribution and atmospheric implications of the gas-phase oxidation of allyl sulfides by OH radicals, *Chemosphere*, 2022, **288**, 132546.

16 I. Barnes, J. Hjorth, N. Mihalapoulos and N. Mihalopoulos, Dimethyl sulfide and dimethyl sulfoxide and their oxidation in the atmosphere, *Chem. Rev.*, 2006, **106**, 940–975.

17 P. H. Wine, N. M. K.reutter, C. A. Gump and A. R. Ravishankara, Kinetics of OH reactions with the atmospheric sulfur compounds H_2S, CH_3SH, CH_3SCH_3, and CH_3SSCH_3, *J. Phys. Chem.*, 1981, **85**, 2660–2665.

18 L. Aristizabal, M. Ángel, C. Orozco, P. Ruiz, J. Quijano and R. Notario, Computational study of the thermal

decomposition and the thermochemistry of allyl ethers and allyl sulfides, *Struct. Chem.*, 2018, **29**, 897–907.

19 M. Izadyar and M. R. Gholami, Substituent effects on the gas phase reactivity of alkyl allyl sulfides, a theoretical study, *J. Mol. Struct.: THEOCHEM*, 2006, **759**, 11–15.

20 Y. Zhao and D. G. Truhlar, The M06 suite of density functionals for main group thermochemistry, thermochemical kinetics, noncovalent interactions, excited states, and transition elements: two new functionals and systematic testing of four M06-class functionals and 12 other function, *Theor. Chem. Acc.*, 2008, **120**, 215–241.

21 S. Grimme, J. Antony, S. Ehrlich and H. Krieg, A consistent and accurate ab initio parametrization of density functional dispersion correction (DFT-D) for the 94 elements H-Pu, *J. Chem. Phys.*, 2010, **132**(15), 154104.

22 H. S. Yu, X. He, S. L. Li and D. G. Truhlar, MN15: a Kohn-Sham global-hybrid exchange-correlation density functional with broad accuracy for multi-reference and single-reference systems and noncovalent interactions, *Chem. Sci.*, 2016, **7**, 5032–5051.

23 D. E. Woon and T. H. Dunning, Gaussian basis sets for use in correlated molecular calculations. V. Core-valence basis sets for boron through neon, *J. Chem. Phys.*, 1995, **103**, 4572–4585.

24 L. Goerigk, A. Hansen, C. Bauer, S. Ehrlich, A. Najibi and S. Grimme, A look at the density functional theory zoo with the advanced GMTKN55 database for general main group thermochemistry, kinetics and noncovalent interactions, *Phys. Chem. Chem. Phys.*, 2017, **19**, 32184–32215.

25 O. N. Ventura, M. Kieninger, A. Katz, M. Vega-Teijido, M. Segovia and K. Irving, SVECV-f12: benchmark of a composite scheme for accurate and cost effective evaluation of reaction barriers, *Int. J. Quantum Chem.*, 2021, **121**, 1–19.

26 T. B. Adler, G. Knizia and H.-J. Werner, A simple and efficient CCSD(T)-F12 approximation, *J. Chem. Phys.*, 2007, **127**, 221106.

27 G. Knizia, T. B. Adler and H.-J. Werner, Simplified CCSD(T)-F12 methods: theory and benchmarks, *J. Chem. Phys.*, 2009, **130**, 054104.

28 K. A. Peterson, T. B. Adler and H.-J. Werner, Systematically convergent basis sets for explicitly correlated wavefunctions: the atoms H, He, B–Ne, and Al–Ar, *J. Chem. Phys.*, 2008, **128**, 084102.

29 M. J. Frisch, G. W. Trucks, H. B. Schlegel, G. E. Scuseria, M. A. Robb, J. R. Cheeseman, G. Scalmani, V. Barone, A. Petersson, H. Nakatsuji, X. Li, M. Caricato, A. V. Marenich, J. Bloino, B. G. Janesko, R. Gomperts, B. Mennucci, H. P. Hratchian, J. V. Ortiz, A. F. Izmaylov, J. L. Sonnenberg, D. Williams-Young, F. Ding, F. Lipparini, F. Egidi, J. Goings, B. Peng, A. Petrone, T. Henderson, D. Ranasinghe, V. G. Zakrzewski, J. Gao, N. Rega, G. Zheng, W. Liang, M. Hada, M. Ehara, K. Toyota, R. Fukuda, J. Hasegawa, M. Ishida, T. Nakajima, Y. Honda, O. Kitao, H. Nakai, T. Vreven, K. Throssell, J. A. Montgomery Jr, J. E. Peralta, F. Ogliaro, M. J. Bearpark, J. J. Heyd, E. N. Brothers, K. N. Kudin, V. N. Staroverov, T. A. Keith, R. Kobayashi, J. Normand, K. Raghavachari, A. P. Rendell, J. C. Burant, S. S. Iyengar, J. Tomasi, M. Cossi, J. M. Millam, M. Klene, C. Adamo, R. Cammi, J. W. Ochterski, R. L. Martin, K. Morokuma, O. Farkas, J. B. Foresman and D. J. Fox, 2019.

30 H.-J. Werner, P. J. Knowles, F. R. Manby, J. A. Black, K. Doll, A. Heßelmann, D. Kats, A. Köhn, T. Korona, D. A. Kreplin, Q. Ma, T. F. Miller, A. Mitrushchenkov, K. A. Peterson, I. Polyak, G. Rauhut and M. Sibaev, The Molpro quantum chemistry package, *J. Chem. Phys.*, 2020, **152**, 144107.

31 F. Neese, The ORCA program system, *Wiley Interdiscip. Rev.: Comput. Mol. Sci.*, 2012, **2**, 73–78.

32 F. Neese, F. Wennmohs, U. Becker and C. Riplinger, The ORCA quantum chemistry program package, *J. Chem. Phys.*, 2020, **152**, 224108.

33 F. Neese, Software update: the ORCA program system—Version 5.0, *Wiley Interdiscip. Rev.: Comput. Mol. Sci.*, 2022, 1–15.

34 Z. Salta, J. Lupi, V. Barone and O. N. Ventura, H-Abstraction from Dimethyl Sulfide in the Presence of an Excess of Hydroxyl Radicals. A Quantum Chemical Evaluation of Thermochemical and Kinetic Parameters Unveils an Alternative Pathway to Dimethyl Sulfoxide, *ACS Earth Space Chem.*, 2020, **4**, 403–419.

35 R. Atkinson, Rate constants for the atmospheric reactions of alkoxy radicals: an updated estimation method, *Atmos. Environ.*, 2007, **41**, 8468–8485.

36 A. Bossolasco, E. P. Faragó, C. Schoemaecker and C. Fittschen, Rate constant of the reaction between CH3O2 and OH radicals, *Chem. Phys. Lett.*, 2014, **593**, 7–13.

37 E. P. Faragó, C. Schoemaecker, B. Viskolcz and C. Fittschen, Experimental determination of the rate constant of the reaction between C2H5O2 and OH radicals, *Chem. Phys. Lett.*, 2015, **619**, 196–200.

38 C. Fittschen, L. K. Whalley and D. E. Heard, The Reaction of CH3O2 Radicals with OH Radicals: a Neglected Sink for CH3O2 in the Remote Atmosphere, *Environ. Sci. Technol.*, 2014, **48**, 7700–7701.

39 I. Barnes, K. H. Becker and N. Mihalopoulos, An FTIR product study of the photooxidation of dimethyl disulfide, *J. Atmos. Chem.*, 1994, **18**, 267–289.

40 C. Bacher, G. S. Tyndall and J. J. Orlando, The Atmospheric Chemistry of Glycolaldehyde, *J. Atmos. Chem.*, 2001, **39**, 171–189.

41 I. Magneron, A. Mellouki, G. Le Bras, G. K. Moortgat, A. Horowitz and K. Wirtz, Photolysis and OH-Initiated Oxidation of Glycolaldehyde under Atmospheric Conditions, *J. Phys. Chem. A*, 2005, **109**, 4552–4561.

42 S. So, U. Wille and G. da Silva, A Theoretical Study of the Photoisomerization of Glycolaldehyde and Subsequent OH Radical-Initiated Oxidation of 1,2-Ethenediol, *J. Phys. Chem. A*, 2015, **119**, 9812–9820.

43 C. B. Rivela, A. L. Cardona, M. B. Blanco, I. Barnes, M. Kieninger, O. N. Ventura and M. A. Teruel, Degradation mechanism of 2-fluoropropene by Cl atoms: experimental

and theoretical products distribution studies, *Phys. Chem. Chem. Phys.*, 2022, **24**, 5094–5108.

44 N. L. Ng, S. S. Brown, A. T. Archibald, E. Atlas, R. C. Cohen, J. N. Crowley, D. A. Day, N. M. Donahue, J. L. Fry, H. Fuchs, R. J. Griffin, M. I. Guzman, H. Herrmann, A. Hodzic, Y. Iinuma, J. L. Jimenez, A. Kiendler-Scharr, B. H. Lee, D. J. Luecken, J. Mao, R. McLaren, A. Mutzel, H. D. Osthoff, B. Ouyang, B. Picquet-Varrault, U. Platt, H. O. T. Pye, Y. Rudich, R. H. Schwantes, M. Shiraiwa, J. Stutz, J. A. Thornton, A. Tilgner, B. J. Williams and R. A. Zaveri, Nitrate radicals and biogenic volatile organic compounds: oxidation, mechanisms, and organic aerosol, *Atmos. Chem. Phys.*, 2017, **17**, 2103–2162.

45 B. H. Lee, C. Mohr, F. D. Lopez-Hilfiker, A. Lutz, M. Hallquist, L. Lee, P. Romer, R. C. Cohen, S. Iyer, T. Kurtén, W. Hu, D. A. Day, P. Campuzano-Jost, J. L. Jimenez, L. Xu, N. L. Ng, H. Guo, R. J. Weber, R. J. Wild, S. S. Brown, A. Koss, J. de Gouw, K. Olson, A. H. Goldstein, R. Seco, S. Kim, K. McAvey, P. B. Shepson, T. Starn, K. Baumann, E. S. Edgerton, J. Liu, J. E. Shilling, D. O. Miller, W. Brune, S. Schobesberger, E. L. D'Ambro and J. A. Thornton, Highly functionalized organic nitrates in the southeast United States: contribution to secondary organic aerosol and reactive nitrogen budgets, *Proc. Natl. Acad. Sci. U. S. A.*, 2016, **113**, 1516–1521.

46 Z. Salta, J. Lupi, N. Tasinato, V. Barone and O. N. Ventura, Unraveling the role of additional OH-radicals in the H-abstraction from dimethyl sulfide using quantum chemical computations, *Chem. Phys. Lett.*, 2020, **739**, 136963.

47 Z. Salta, M. E. Segovia, A. Katz, N. Tasinato, V. Barone and O. N. Ventura, Isomerization and Fragmentation Reactions on the $[C_2SH_4]$ Potential Energy Surface: The Metastable Thione S -Methylide Isomer, *J. Org. Chem.*, 2021, **86**, 2941–2956.

48 Z. Salta, M. Vega-Teijido, A. Katz, N. Tasinato, V. Barone and O. N. Ventura, Dipolar 1,3-cycloaddition of thioformaldehyde S-methylide (CH_2SCH_2) to ethylene and acetylene. A comparison with (valence) isoelectronic O_3, SO_2, CH_2OO and CH_2SO, *J. Comput. Chem.*, 2022, **43**(21), 1420–1433.

49 T. Berndt, J. Chen, K. H. Møller, N. Hyttinen, N. L. Prisle, A. Tilgner, E. H. Hoffmann, H. Herrmann and H. G. Kjaergaard, SO2 formation and peroxy radical isomerization in the atmospheric reaction of OH radicals with dimethyl disulfide, *Chem. Commun.*, 2020, **56**, 13634–13637.